CHAPTER 2

Principle and Basic Instrumentation of Mass Spectrometry

The purpose of this chapter is to introduce the fundamental concept of mass spectrometry and explain about the quadrupole mass spectrometers and basic instrumentation of mass spectrometry.

2.1 Fundamental Concept of Secondary Ion Mass Spectrometry (SIMS)

Secondary Ion Mass Spectrometry is a method for analyzing the elemental and the chemical composition of the material. It has been available for forty years or more, useful for characterizing the top few micrometers of material samples. Primary ions of energy 0.5 – 30 keV, commonly Ar^+, O^-, O_2^+,Cs^+, Ga^+ and Xe^+, are used to erode the sample surface, which leads to the ejection (or *sputtering*) of both neutral and charged (+/-) species from the surface. The ejected species may include atoms, clusters of atoms and molecular fragments call the secondary ions. The secondary ions are extracted from the surface by an electric field and their energy and mass are analyzed. The secondary ions are detected and the resulting secondary ion distribution is displayed as a function of mass, surface location, a function of depth (called a depth profile), or for identifying molecular species. There are a number of different variants of the technique Static SIMS is used for sub-monolayer elemental analysis. Dynamic SIMS is used for obtaining compositional information as a function of depth below the surface. Imaging SIMS is used for spatially-resolved elemental analysis. All of these variations on the technique are based on the same basic physical process.

The main elements of a SIMS system are (i) a primary ion source, (ii) optics to transfer the primary ions to the target surface and to collect secondary ion from the surface and direct them to, (iii) a mass spectrometer (such as a quadrupole mass spectrometer) and (iv) ion detector and electronics as shown in Figure 2.1. The signal due to the detected secondary ions may be presented as a function of (a) the ion mass, (b) the duration of ion bombardment.

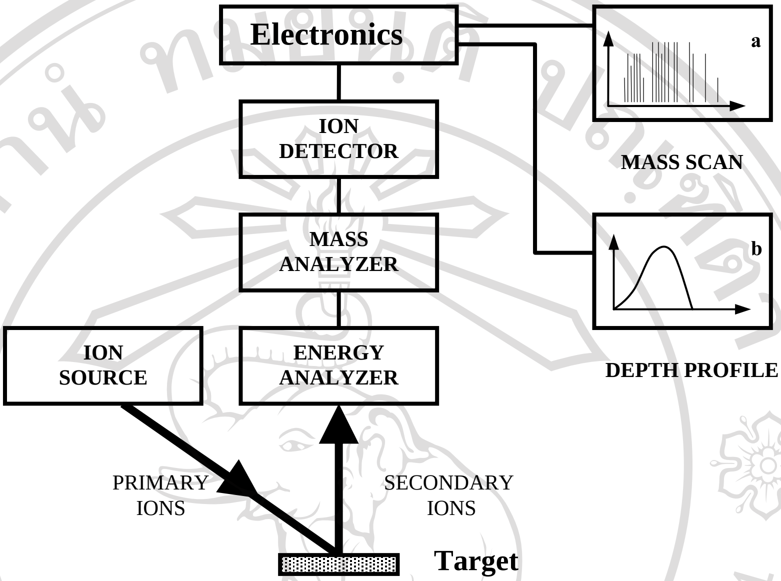

Figure 2.1 Schematic representation of the main components of a SIMS experiment (McEwen and others, 1990).

There are many other techniques available for elemental analysis. Table 2.1 gives a short comparison of the most relevant analytical capabilities of the MeV ion beam analysis techniques for elemental analysis with those of Rutherford Backscattering Spectrometry (RBS), Proton Induced X-ray Emission (PIXE), Nuclear Reaction Analysis (NRA) and Elastic Recoil Detection Analysis (ERDA). The values given in this table are only approximate, since the capabilities of each technique vary widely, depending on operating condition and the analytical requirement of different samples.

Table 2.1 Comparison of ion beam analysis techniques for elemental analysis (Breese and others, 1996)

Method	Measured signal	Depth resolution (nm)	Detectable elements (Atomic number)	Detection sensitivity (wppm)	Quantitivity (%)
RBS	Backscattered incident ion	0.02	> 2	1	3
PIXE	X - ray	5	> 11	0.1	5
NRA	Charge particle reaction products	0.005	All low Z	0.01	3
ERDA	Forward scattered sample ions	0.005	< 15	500	3
SIMS	Sample ions	0.005	All	0.001-10	50

2.1.1 Ion beam sputtering of solid target

Sputtering is the erosion of a sample by energetic particle bombardment. When a primary ion with certain energy, a mass, and a charge state bombards a solid target surface and then penetrates inside the solid, various physical processes occur. The bombarding primary ion beam produces monatomic and polyatomic particles of sample material and resputtered primary ions, along with electrons and photons. In the sputtering process, the bombarding ion transfer energy in collisions to target atoms which recoil with sufficient energy (called recoil atoms) to generate other recoils. Some of these backward recoils will approach the surface with enough energy to escape from the sample. The collision cascade model as shown in Figure 2.2 has the best success at quantitatively explaining how the primary beam interacts with the sample atoms. In this model, a fast primary ion passes energy to target atoms in a series of binary collisions. Energetic target atoms (recoil atoms) collide with more target atoms. Target atoms which have the energy more than surface binding energy (SBE) recoil back through the sample surface constitute sputtered material. The sputtered atoms (secondary atoms) carry negative, positive, and neutral charges and they have kinetic energies that range from zero to several hundred eV.

Primary ions are implanted and mixed with sample atoms to depths of about 1 to 10 nm. The sputter rates in typical SIMS experiments vary between 0.5 to 5 nm/s. The sputter rates depend on primary beam intensity, sample material, and crystal orientation.

The sputtering yield *Y* is defined as the ratio of an average number of sputtered atoms to the number of incident particle. It depends on structure and composition of the target material, parameters of the incident ion beam and experimental geometry. Generally, it can be written as follows:

$$D = \frac{YF}{N},$$

where *D* is sputtered thickness, *N* is a target atom density and *F* is an ion fluence.

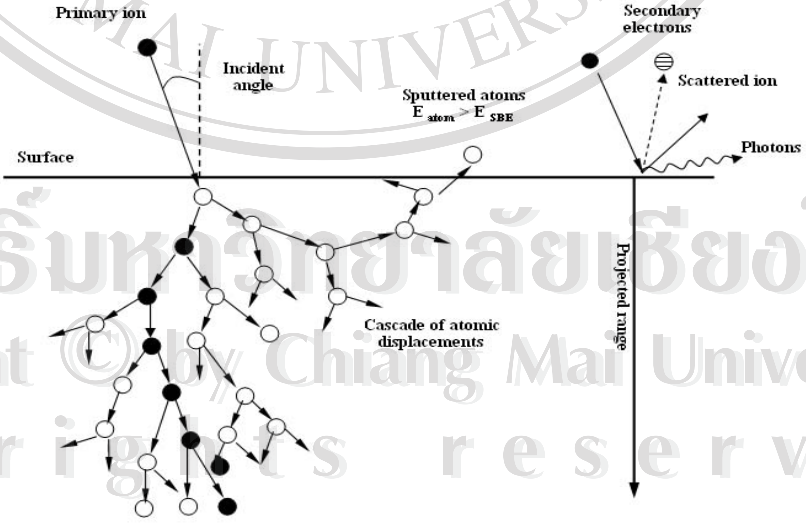

Figure 2.2 Schematic drawing of ion-solid sputtering process (Yu, 1997).

2.1.2 Kinetic energy distribution of the secondary ions

The sputtering process produces secondary ions with a range of kinetic energies (so called translational). The energy distributions are distinctly between for atomic and molecular ions. Molecular ions have relatively narrow translational energy distributions since they have kinetic energy in internal vibration and rotational modes. Atomic ions have all kinetic energy in translational modes. Figure 2.3 shows typical kinetic energy distributions for monatomic $\left(M_1^+\right)$, diatomic $\left(M_2^+\right)$, and triatomic $\left(M_3^+\right)$ ions. The intensity of monatomic is higher than diatomic and triatomic at the same energy (energy >2 eV).

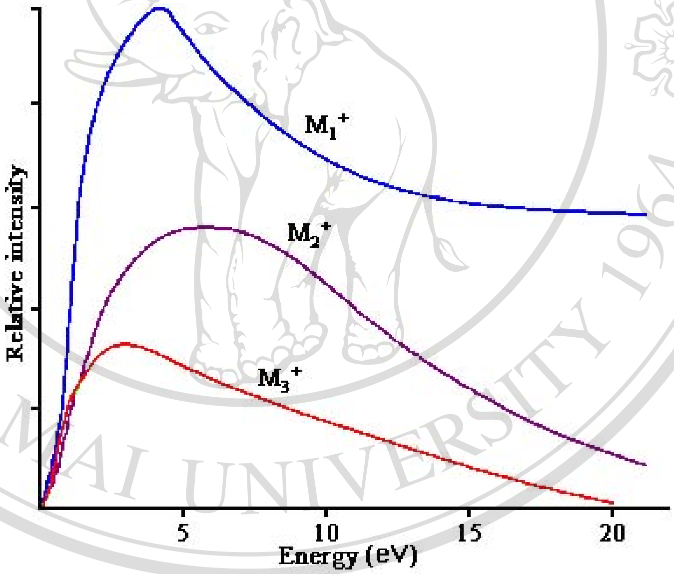

Figure 2.3 Typical kinetic energy distribution of the sputtered monatomic, diatomic and triatomic ion (Fleming, 1995).

2.1.3 Separation of the secondary ions

For conventional SIMS, the secondary ions are generated continuously by using a static primary beam, the different ion species are detected sequentially, e.g., in a magnetic mass or the quadrupole spectrometer. At a given instant, only secondary ions of the selected *m/z* ratio reach the detector, thus most secondary ions are not measured or there are lost in the measurement. Time of fight (TOF)-SIMS is contrary because this spectrometry allows measuring all secondary ions with one polarity simultaneously. The sample is bombarded with a short-time primary ion pulse with typical lengths between few nanoseconds to several hundred picoseconds. This is repeated every few hundred microseconds to the order of microseconds.

2.2 Basic Instrumentation of Mass Spectrometry

The mass spectrometry consists of three major components; ion source, mass analyzer and ion detector. The details each of the basic components are briefed as follows.

2.2.1 Ion Source

The region of the mass spectrometer where ions are generated is called the ion source. There are many techniques that can be applied to ionize molecules of the vaporized sample such as electron impact ionization (EI), chemical ionization (CI), surface ionization, field desorption and secondary ionization (Howe and others, 1981). In this section, electron impact ionization and chemical ionization (two of the more important methods) are briefly discussed.

- **Electron-impact ionization**

The electron-impact ionization is the most commonly used ionization method as shown in Figure 2.4. An electron beam, usually generated from tungsten filament, is used to ionize gas-phase atoms or molecules. Ions are formed during collision of the electron beam and sample molecules. This reaction is represented as follows;

$$M + e^- \rightarrow M^+ + 2e^- .$$

Here M represents the analyze molecule and M+ is its molecular ion. The positive ions are accelerated by an electric field and passed into a mass analyzer; ions of different mass-to-charge ratio (*m/z*) can be collected and measured.

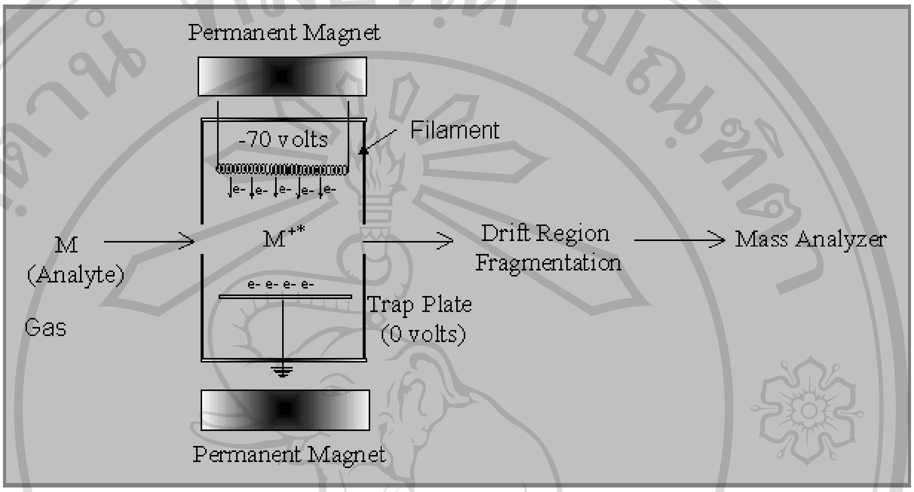

Figure 2.4 Schematic diagram of electron impact ionization (Nobel Foundation, 1997).

- **Chemical ionization**

In chemical ionization, a small amount of gaseous atoms is ionized by collision with ions produced by electron bombardment of the reagent gas as shown in Figure 2.5. The reaction is represented as follows:

$$M + \left[reagent\ \ gas + H\right]^{+} \rightarrow \left[M + H\right]^{+} + reagent\ \ gas\ ,$$

$$M + \left[reagent\ \ gas - H\right]^{-} \rightarrow \left[M - H\right]^{-} + reagent\ \ gas\ .$$

The gas-phase chemical reactions result in the removal or donation of a charged species (generally H+) from the reagent gas to the analyte to yield a pseudo-molecular ion (positively or negatively charged). Typical reagent gases used in CI are methane, isobutane, ammonia, and hydrogen.

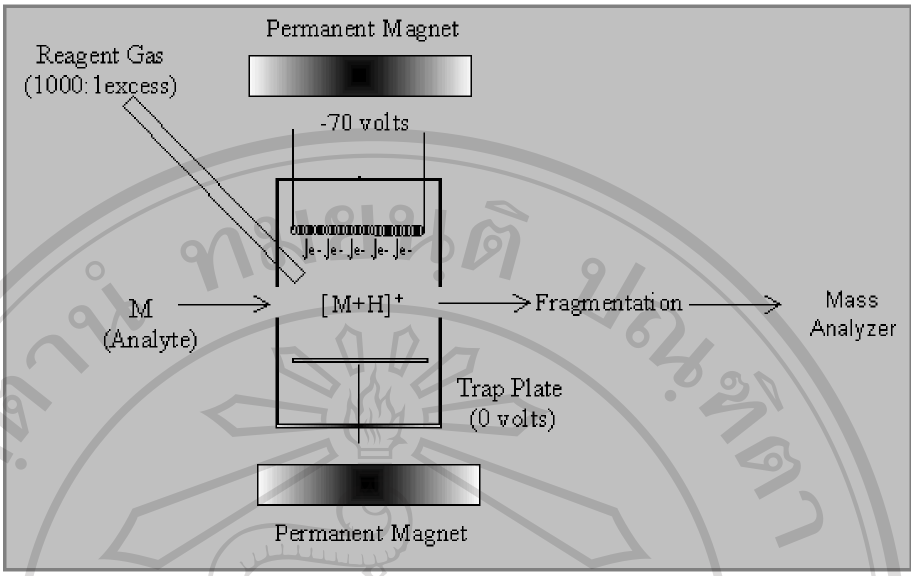

Figure 2.5 Schematic diagram of chemical ionization (Nobel Foundation, 1997).

2.2.2 Mass Analyzing techniques

The most important part of the secondary ion mass spectrometry is the mass analyzer. These mass analyzers separate ions according to their mass-to-charge ratio, may take several forms. The several methods which are commonly used for analysis are (i) deflection of the secondary ions in electric field and magnetic field or both, (ii) penetration through the quadrupole field (iii) measurement of the time-of-flight and etc. The methods are described below.

- **Deflection of the secondary ions**

The ionized molecules or atoms of different masses from the source are separated by the electric field and magnetic field. If a charged particle with mass m moves in a velocity $\vec{v}$ through the electric field $\vec{E}$ and magnetic field $\vec{B}$. The Lorenz force $\vec{F}$ is given by

$$\vec{F} = ze\left(\vec{E} + \left(\vec{v} \times \vec{B}\right)\right), \qquad (2.1)$$

where z is the number of such charges and e is the charge of the electron. The force acting on a moving charge particle is always parallel and perpendicular to the direction of the electric field and magnetic field, respectively. The charged particle traveling under electric field produces a displacement s, as shown in Figure 2.6, is given by

$$s = \frac{zex^2}{2mv}E, \tag{2.2}$$

where x is the distance inside the electric field and m is the mass of charged particle.

If the charged particles are applied to a region where only a magnetic field exists, a circular motion with radius r is produced and this is the based of the deflection type mass spectrometry. Hence, from Newton's second law of motion,

$$F = \frac{mv^2}{r} = zevB. \tag{2.3}$$

The kinetic energy of the charged particle is independent to their masses, is given by

$$T = \frac{1}{2}mv^2 = zeV, \tag{2.4}$$

where V is an accelerated voltage to the charged particle. Combining Equations (2.3) and (2.4) leads to

$$\frac{m}{z} = \frac{B^2r^2e}{2V}. \tag{2.5}$$

From Equation (2.5) it is evident that, at a given magnetic field strength and accelerating voltage, ions of a given m/z value will follow a particular path of radius r and that the ions of various m/z values may be progressively transmitted through the magnetic field and the slit (Figure 2.7) either by varying B at constant V or by varying V and constant B. The former possibility is called the magnetic scanning and the latter is the electric scanning.

The mass resolution of this instrument is constant over the detectable mass range. The sensitivity depends on the efficiency of the ion production and the slit width which determines the transmission of the ions to the detector while the mass range is determined by the strength of the magnetic field.

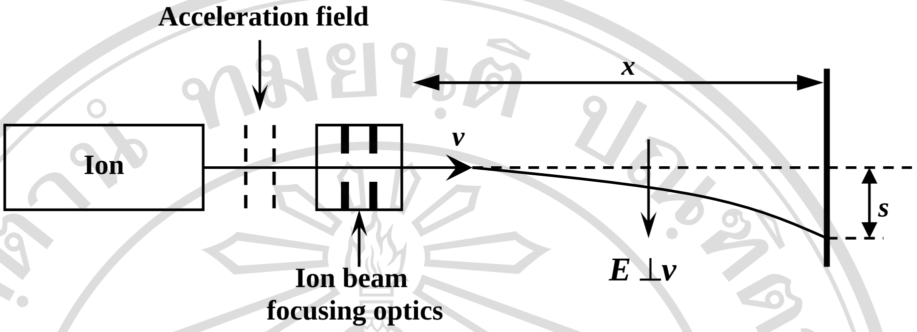

Figure 2.6 The path of the ion under an electric field (Piyadasa, 2000).

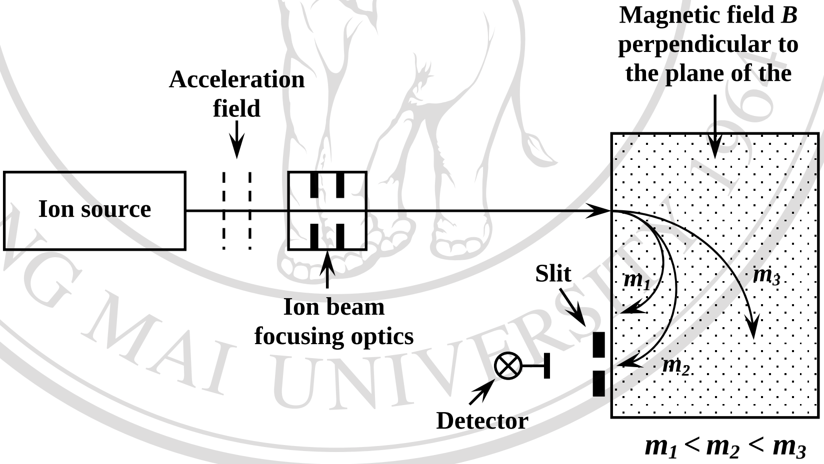

Figure 2.7 The paths of m_1, m_2 and m_3 in magnetic field (Piyadasa, 2000).

- **Quadrupole Analyzer**

The quadrupole is a device that utilizes the stability of the trajectories in oscillating electric field to separate an ion with a certain *m/z* ratio, consisting of four precisely parallel rods. The quadrupole instrument is shown in Figure 2.8. Only ions of a certain *m/z* ratio pass through the quadrupole filter and then go to the detector and all other ions are thrown out of their original path. The principle of the quadrupole is required to be described in section 2.3. Quadrupole analyzers have become the most widely used mass analyzer in mass spectrometry because of their light weight, purely electronic scanning, linear mass scale and apparent simplicity.

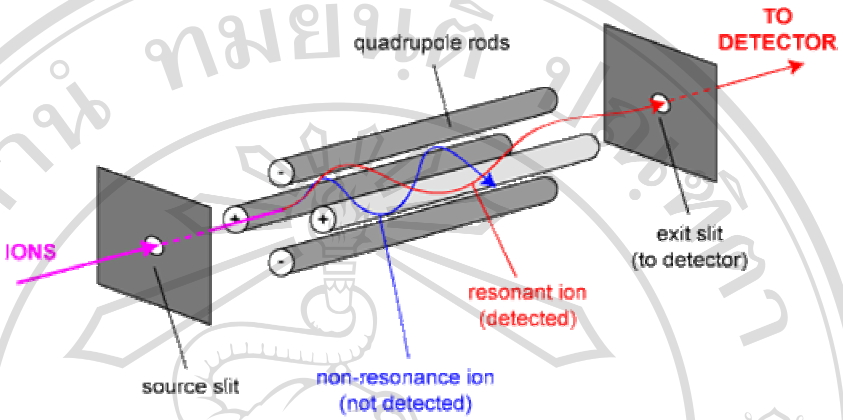

Figure 2.8 Quadrupole instrument made of the source, the quadrupole cylindrical rods and the detector (Gates, 2004).

- **Time-of-flight mass analyzer**

Ions with different mass are given equal energy. That cause different ions have different velocities and hence different times of flight over a given distance. If there is a fixed distance of travel of the ions, the time of their travel will vary with their mass, the lighter masses traveling more rapidly reaching the detector in a shorter of time. The essential component of this type of analyzer include (1) ions are introduced such as pulsed ion source, (2) the acceleration region which is considered as the start signal for time measurement, (3) the drift region (flight tube) before reaching the detector which detects the ions and produces the stop timing signal of the measurement and (4) a sensitive fast response ion detector. Figure 2.9 is a schematic diagram of time-of-flight spectrometer. The time different between start and stop signal is called time-of-flight (TOF) and is proportional to the square root of the *m/z* ratio of the ions.

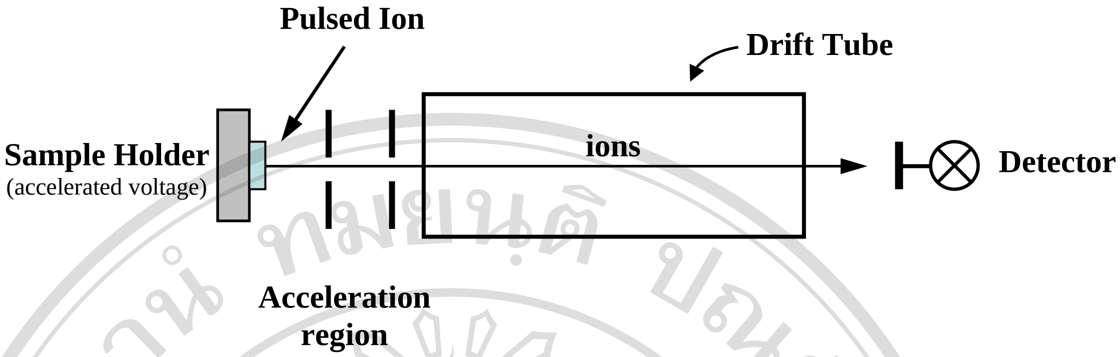

Figure 2.9 Schematic diagram of time-of-flight spectrometer.

2.2.3 Ion Detection

The detection is the final step in ion maneuvering process in a mass analyzer. A Faraday cup or plate used in conjunction with a sensitive electronic amplifier represents the simplest, cheapest, and most reliable means for detecting the ion beams emerging from the exit aperture of the quadrupole. The relatively high noise level and the slow response of this technique can be improved by using an electron multiplier as the detector in place of the Faraday cup. The multiplier becomes, in effect, the first stage of the signal amplifier where full advantage can be taken of its extremely low noise level and its fast response.

- **The Faraday cup**

A Faraday cup or a simple plate collector is just an electrode from which electrical current is measured while an ion impinges on it. The shape of the collector is usually designed to minimize the escape of any reflected and/or secondary electrons that would alter the current measurement. A schematic diagram of the Faraday cup is shown in Figure 2.10.

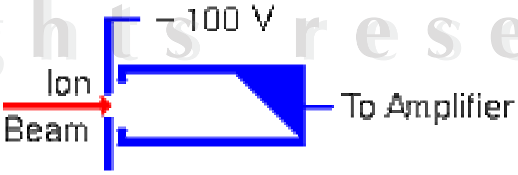

Figure 2.10 Schematic representation of a Faraday cup (Fleming, 1995).

- **The electron multiplier**

The signal-to-noise ratio and the speed of response of the detector can be improved by replacing the Faraday cup with an electron multiplier. The signal-to-noise ratio is the ratio of the magnitude of the signal to that of the background noise detected (Storey, 1992). Signal can increase by use electron multiplier. This introduces a pre-amplifier with a current gain in the range 10^5 to 10^7. An electron multiplier consists of a cathode and series of electrodes called dynodes, each connected along a resistor string. The dynode potentials differ in equal steps along the chain.

When a charge particle strikes the cathode it produces secondary electrons. The secondary electrons are accelerated and allowed to impinge upon another dynode where each electron produces more secondary electrons. The dynode acceleration potential controls the electron gain. Finally all electrons are collected on the anode. In this way, a large electron current can be obtained for each charge particle collected at the cathode detector. Figure 2.11 schematically shows such a multiplier.

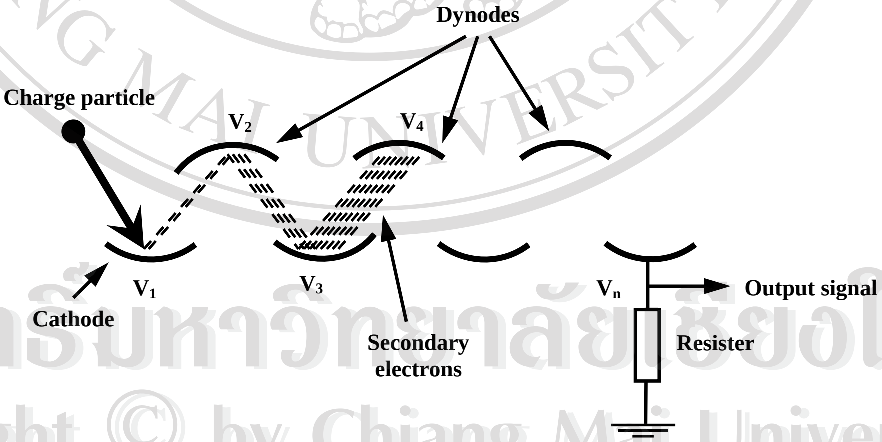

Figure 2.11 Schematic representation of an electron multiplier.

2.3 Quadrupole Mass Spectrometers

The quadrupole mass analyzer was developed in parallel with the quadrupole ion trap by the third Nobel Prize winning mass spectrometry pioneer, Wolfgang Paul (Paul and Steinwedel, 1953). The quadrupole analyzer is a device that uses the stability of the trajectory in oscillating electric fields to separate ions, allow ions of a chosen mass to *m/z* ratio to pass to it while rejecting all other, consisting of four precisely parallel metal rods. A schematic diagram of the positioning of the four long, parallel electrodes is shown in Figure 2.12. They are sets of rectangular hyperbolae in the *xy* plane with, geometrically, four rods symmetry about the *z* axis. The distance between opposite electrodes is $2r_o$. Two opposite rods have an applied positive potential $+\Phi_o$ (see section 2.3.2) and the other two rod has a negative potential $-\Phi_o$. Although the electrodes are shown to have a uniform hyperbolic cross section, cylindrical rods can be used if they are properly spaced.

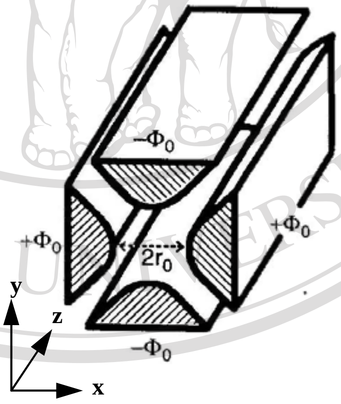

Figure 2.12 The ideal quadrupole mass filter electrodes having hyperbolic cross section (Hoffmann and Stroobant, 2001).

2.3.1 The quadrupole field

A quadrupole field *E* is expressed by its linear dependence on the co-ordinate position. In the Cartesian co-ordinate *x, y,* and *z* (Dawson, 1995)

$$E = E_0(\lambda x + \sigma y + \gamma z), \tag{2.6}$$

where λ, σ, and γ are weighting constants and E_o is a position-independent factor which may be a function of time. For an ion is traveling in a quadrupole field, the force acting upon it, *ZeE*, increases according to the displacement of the ion from zero. Hence, from Laplace's equation,

$$\nabla \cdot E = 0\,, \tag{2.7}$$

so that $\lambda + \sigma + \gamma = 0$. The simplest ways of satisfying Equation (2.7) are evidently

$$\lambda = -\sigma; \gamma = 0 \tag{2.8}$$

and

$$\lambda = \sigma; \gamma = -2\sigma\,. \tag{2.9}$$

To express these conclusions by determine the form of the potentials to be applied. This is done by integration, since $-\left(\partial \Phi / \partial x\right) = E_x$ etc. The potential Φ can suitably be expressed as:

$$\Phi = -\frac{1}{2} E_0 \left(\lambda x^2 + \sigma y^2 + \gamma z^2\right) \tag{2.10}$$

Consider first, the relation given in Equation (2.8). Then

$$\Phi = -\frac{1}{2} E_0 \lambda \left(x^2 - y^2\right), \tag{2.11}$$

The equipotential lines of quadrupole field are shown in Figure 2.13.

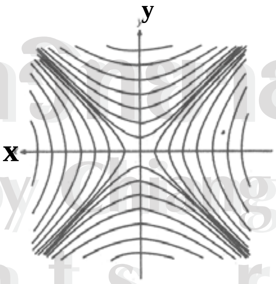

Figure 2.13 Equipotential lines for a quadrupole field (Dawson, 1995).

The potential and the minimum distance between opposite rods are Φ_o and $2r_o$, respectively. Equation. (2.11) becomes:

$$\Phi = \frac{\Phi_0\left(x^2 - y^2\right)}{r_0^2}\ , \tag{2.12}$$

since $$\lambda = -\frac{2}{r_0^2}\ .$$

2.3.2 The applied potential

The ions accelerators along the *z*-axis enter the space between the quadrupole rods and maintain their velocity along this axis. However, they are submitted to accelerations along *x* and *y* that result from the forces induced by the electric fields. The equation of ion motion are given by

$$F_x = -ZeE_x = m\frac{d^2x}{dt^2} \tag{2.13}$$

and $$F_y = -ZeE_y = m\frac{d^2y}{dt^2} \tag{2.14}$$

That is $$\frac{d^2x}{dt^2} + \left(\frac{2Ze}{mr_0^2}\right)\Phi_0 x = 0 \tag{2.15}$$

$$\frac{d^2y}{dt^2} - \left(\frac{2Ze}{mr_0^2}\right)\Phi_0 y = 0\ . \tag{2.16}$$

Equations (2.15) and (2.16) give the ion motion in the *x-z* and *y-z* planes. The potential between the opposite rods Φ_o has usually been ($U - V\cos\omega t$). That are a *dc* voltage (*U*), a radio frequency (*rf*) in the term of $V_o\cos\omega t$ and angular frequency ω (2πf). In principle, for a given potential field configuration, it is only the mass and ionic charge that determines whether an ion trajectory is stable of unstable. If the particle injected into the quadrupole are positive ions, the potential lines established by the *dc* voltage alone will have some focusing effect toward the z axis, and a slightly divergent ion constrained to the *x-z* plane will undergo simple harmonic oscillations. The addition of the *rf* field will then superpose a high-frequency oscillation. The *dc* voltages in the *y* electrodes tend to cause some defocusing, but the superposition of an *rf* voltage, which is usually high compared to the *dc* potentials, has the effect of a focusing action toward the *z* axis.

Also, in practical designs, cylindrical rods are chosen instead of hyperbolic-contoured surfaces because of the ease of manufacture. The cylindrical rod assembly provides approximately the same field distributions, provided the radius of the rods *r* relative to the value of r_o is related by

$$r_o = \frac{r}{1.147}. \tag{2.17}$$

2.3.3 The equation of motion

Returning to the equations of motion for the mass filter, consider also the monopole and the three-dimensional quadrupole ion trap. For the monopole, the equations of motion of the ions are described by following three equations:

$$\frac{d^2x}{dt^2} + \frac{2Ze}{mr_0^2}(U - V\cos\omega t)x = 0, \tag{2.18}$$

$$\frac{d^2y}{dt^2} - \frac{2Ze}{mr_0^2}(U - V\cos\omega t)y = 0, \tag{2.19}$$

and

$$\frac{d^2z}{dt^2} = 0. \tag{2.20}$$

The trajectory of an ion will be stable if the value of *x* and *y* never reaches r_o, i.e. if it never hits the rods. To obtain the values of either *x* or *y* during the time, these equations need to be integrated. The following equation was established in 1866 by the physicist Mathieu in order to describe the propagation of waves in membranes. In order to put Equations (2.18) and (2.19) into the form of Mathieu's equation,

$$\frac{d^2u}{d\xi^2} + (a_u - 2q_u\cos 2\xi)u = 0, \tag{2.21}$$

where *u* represents either *x* or *y*

The dimensionless parameters define as follows:

$$\xi = \frac{\omega t}{2}, \tag{2.22}$$

$$a_u = a_x = -a_y = \frac{8zeU}{m\omega^2 r_o^{\ 2}}, \tag{2.23}$$

and
$$q_u = q_x = -q_y = \frac{4zeV}{m\omega^2 r_o^{\ 2}}. \tag{2.24}$$

Then, the Mathieu’s equations for the motions in x and y directions are

$$\frac{d^2 x}{d\xi^2} + \left(a_x + 2q_x \cos 2\xi\right)x = 0 \tag{2.25}$$

and
$$\frac{d^2 y}{d\xi^2} - \left(a_y + 2q_y \cos 2\xi\right)y = 0. \tag{2.26}$$

Solution of Equation (2.21) is (Dawson, 1995)

$$u = \alpha' e^{\mu\xi} \sum_{n=-\infty}^{\infty} C_{2n} e^{2in\xi} + \alpha'' e^{-\mu\xi} \sum_{n=-\infty}^{\infty} C_{2n} e^{-2in\xi} \tag{2.27}$$

where α' and α'' are integration constants depend on the initial condition. The constants C_{2n} and μ depend on the value of a_u and q_u which not depend on the initial conditions. Then we have the nature of the ion motion depends on a_u and q_u.

Equation 2.27 have two types depend on the nature of μ.

1. Stable solutions are those where μ remains finite when $\xi \rightarrow \infty$ provide the value of x and y dose not exceed r_0.
2. Unstable solution where μ increase without limit when $\xi \rightarrow \infty$ or some conditions the value of x and y dose not exceed r_0. The particle will be lost.

The limited range of values of a_u and q_u when the amplitude of an ion oscillation is remain bounded or the value of μ is finite (the stable solution) will discuss in section 2.3.4

2.3.4 Stability diagram

From section 2.3.3, consider the value of μ to get the stable solution. There are four possibilities of μ.

1. μ is real and non-zero. Instability arises from the $e^{\mu\xi}$ or $e^{-\mu\xi}$ factor.
2. $\mu = i\beta$ is purely imaginary and β is not a whole number. These solutions are the periodic stable.
3. μ is a complex number. The solutions are not stable.
4. $\mu = im$ is purely imaginary and m is an integer. The solutions are periodic but not stable. For m = 2n the periodicity is π in ξ and for m = 2n + 1 the periodicity is 2π. These solutions are called Mathieu function of integral order, form the boundaries in a and q space between stable and unstable regions.

Since μ depends on a_u and q_u then the conditions of stability can be represented on an a–q diagram or stability diagram. The stability diagram of Equations 2.25 and 2.26 are shown in Figure 2.14(a) and Figure 2.14(b), respectively. The shade areas are the stable regions of the trajectory.

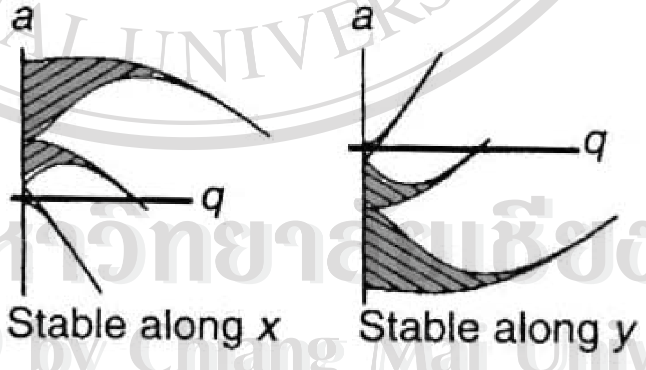

Figure 2.14 (a) The a-q diagram for the Mathieu equation in x direction. (b) The a-q diagram for the Mathieu equation in y direction (Hoffmann, 2001).

Figure 2.15 shows the overlay of two diagrams in Figure 2.14(a) and Figure 2.14(b) represent the allowed regions where the ions will have stable trajectories according to the *x* and *y* axes simultaneously. The stable regions or stability areas are labeled *A* to *D* and are circled. The area *A* is used commonly in mass spectrometers.

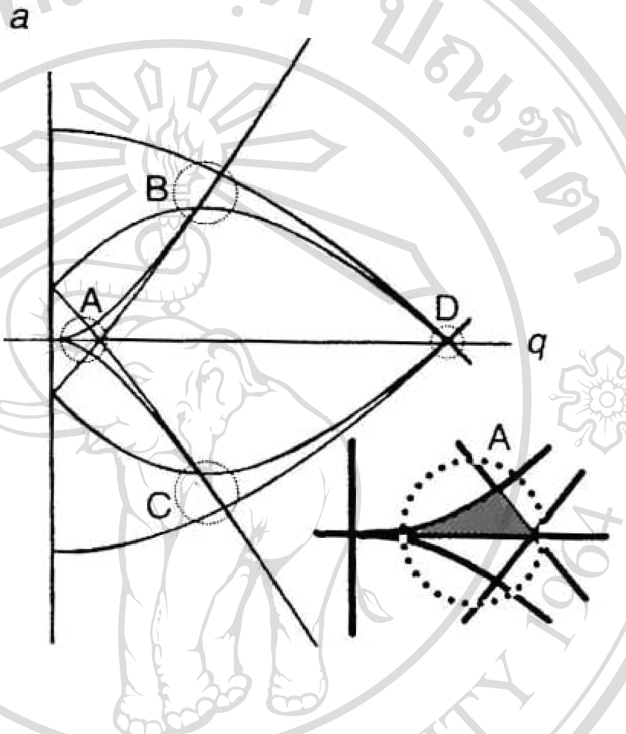

Figure 2.15 Stability areas for an ion along *x* and *y*. The four stability areas are labeled *A* to *D* and are circled (Hoffmann, 2001).

From Equations 2.23 and 2.24 we can deduce

$$U = a_u \frac{m}{z}\frac{\omega^2 r_o{}^2}{8e}, \qquad V = q_u \frac{m}{z}\frac{\omega^2 r_o{}^2}{4e} \tag{2.28}$$

$$\frac{a}{q} = \frac{2U}{V} \tag{2.29}$$

For an ion of any mass, *x* and *y* can be determined during a time span as a function of *U* and *V*. In the stability areas which are shown in Figure 2.16, the values of *U* and *V* are such that *x* and *y* do not reach values above or equal to r_o. There is a region of stable oscillations, where the amplitude remains finite for all values of time.

This is the region enclosed in the triangular-shaped wedge, outside of this region of stable oscillations, the amplitude increases exponentially toward infinity. Only ions of m/z values given by the appropriate a_u and q_u, U and V, ω and r_o will pass through the quadrupole analyzer without striking the electrodes and thereby reach the detector. The apparent possibility of an infinitely high resolution as the scan line approaches the stability tip at the point $a = 0.23699$ and $q = 0.70600$.

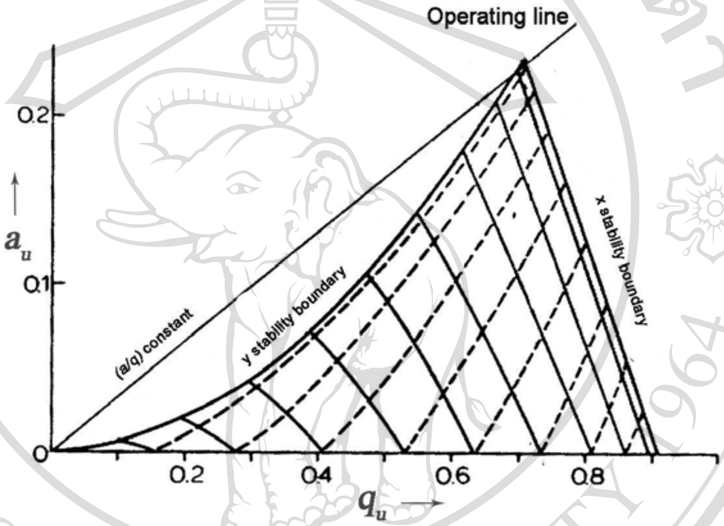

Figure 2.16 The stability region normally used in mass filter operation showing a typical operating line (Dawson, 1995).

To gain some idea, consider the OC line of $a/q = 0.306$ or $U/V = 0.153$ in Figure 2.17. For V = 1,000 volts (then U = 0.153 x 1000 = 153 volts), radius of rods r = 4 mm and frequency of 2 MHz. The point m_1/z (a=0.213) is for a mass to charge ratio of 295 and have the stable trajectory. Points m_2/z = 353 (a = 0.178) and m_3/z = 452 (a = 0.139) but both of them can not pass through the quadrupole because they are in unstable region. Equation 2.28 predicts that point D (a = 0.232) correspond to an ion of m/z = 271 and G (a = 0.202) to m/z = 311. For these parameter values all m/z between 271 and 311 will be transmitted through the quadrupole.

In order to achieve high resolution, measurement must be made near the apex region of the curve (OA line) at *a* = 0.237 and *q* = 0.706. At the same parameter values only ion of *m/z* 265 will be transmitted.

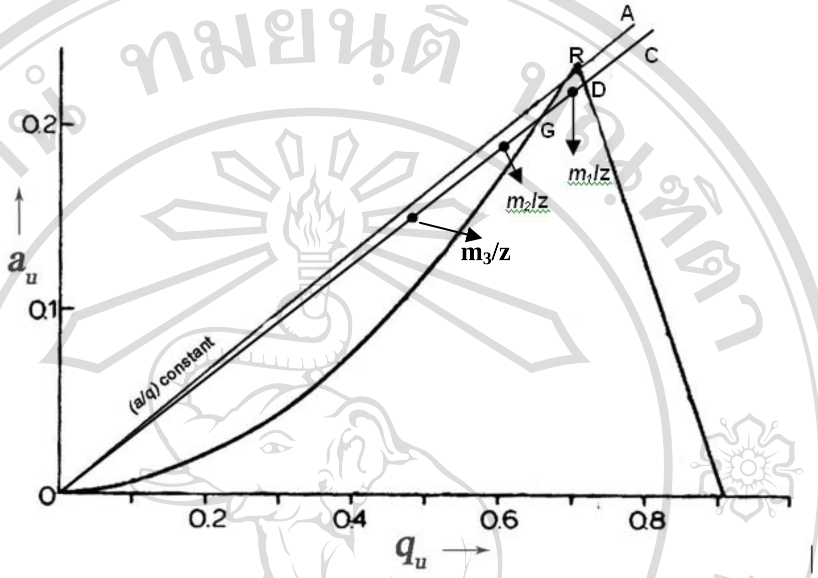

Figure 2.17 Relation of *a* and *q* for quadrupole mass apectrometer. The higher slope the higher resolution.

2.3.5 Mass range and resolution

The two main characteristics of a quadrupole are the mass range and the maximum resolution. The mass range determines the highest mass in atomic mass units (amu) that can be measured. The resolution (R) is ion separation power of a mass spectrometer to yield distinct signals for two ions with a small mass difference as shown in Figure. 2.18. The maximum resolution and the mass range are depending on five basic parameters. The maximum resolution depends on length of the rods, the rf supply frequency and the ion injection energy. The mass range depends on diameter of the rods, the maximum supply voltage to the rods and the same with the resolution, the rf supply frequency. Figure 2.19 shows the relationship of resolution and mass range to the five main parameters.

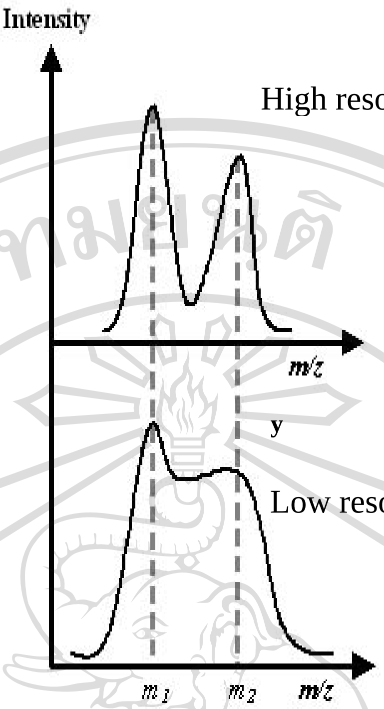

Figure 2.18 Diagram showing the peak with high resolution and low resolution (Hoffmann, 2001).

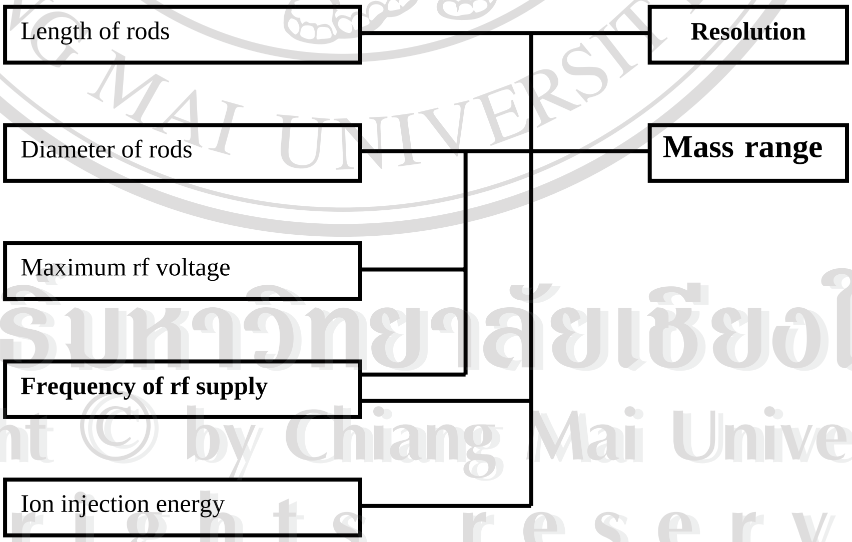

Figure 2.19 Relationship of resolution and mass range to the instrument parameter.

The maximum mass M_m is (Dawson, 1995)

$$M_m = \frac{7 \times 10^6 V_m}{f^2 r_0^2} \tag{2.30}$$

and resolution is

$$R = \frac{M}{\Delta M} \tag{2.31}$$

where V_m is the rf maximum voltage applied between adjacent rods, f is the *rf* supply frequency, r_o is the minimum radius between opposite rods in meters. ΔM is the width of the peak at mass M. Figure 2.20 shows the peaks at different ΔM. If the peak of mass M has ΔM equal to 3 amu and another peak at mass $M+1$ has ΔM equal to 3 amu, too. The spectrum that we get will not resolve clearly as shown in Figure 2.21

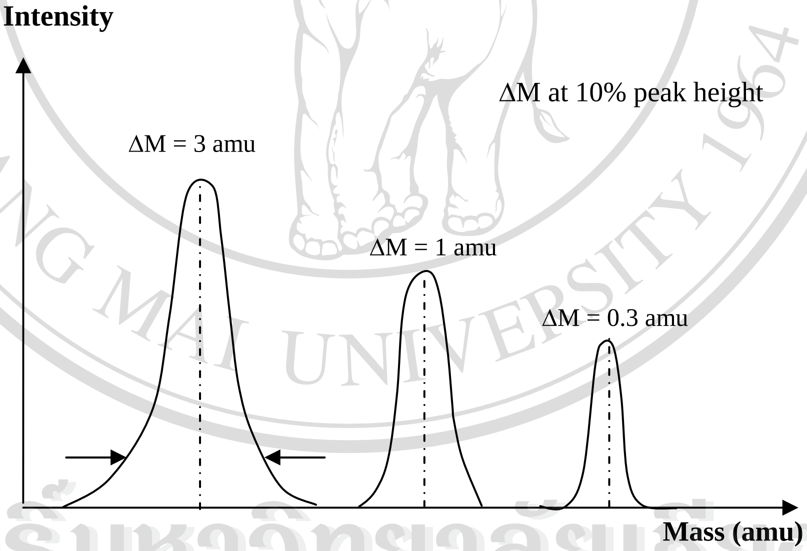

Figure 2.20 Peaks at different ΔM

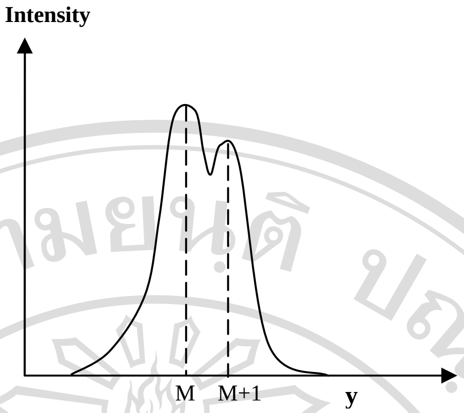

Figure 2.21 Peak of mass M and M+1 with ΔM = 3 amu.

ΔM in amu is

$$\Delta M = \frac{4\times 10^{9}E_z}{f^2L^2}, \tag{2.32}$$

where E_z is the ion injection energy in eV and L is the length of the quadrupole rods in meters. The maximum mass and the maximum resolution are measure in amu. For the majority of instruments designed and operated to the present data, the available choice of V_m and r_o has been relatively limited. Vm is limited by the difficulties inherent in the design of very stable high voltage a.c. generators and r_o by the problem of maintaining a high mechanical accuracy in manufacture of the rod assembly at a reasonable cost which both very large and very small instruments. There is no practical lower limit to the frequency, so that by adjustment of this parameter, the mass range can be extended indefinitely. By eliminating f in Equations (2.30) and (2.32) gives the following relationship between mass and ΔM.

$$\Delta M = \frac{570r_0^2V_zM_m}{L^2V_m} \tag{2.33}$$

The peak width ΔM is directly proportional to maximum mass and independent of the operating frequency, then theoretical maximum resolution is

$$\frac{M_m}{\Delta M} = \frac{L^2V_m}{570E_zr_0^2}. \tag{2.33}$$

2.4 Analytical Information

Several types of analytical information can be generated from the SIMS system**.** The secondary ion can be displayed as a function of mass (mass spectrum), surface location (image) or depth into the sample (depth profile). This section will describe the mass spectrum and the depth profile.

2.4.1 Mass spectrum

A mass spectrum shows the elemental and ion composition (positive and negative) of analyzed surface by the ion signal while scanning a range of mass-to-charge (m/z) ratios. The mass spectrum detects both atomic and molecular ions from the topmost layer of the surface. Figure 2.22 shows mass spectra from polytetrafluoroethylene (PTFE).

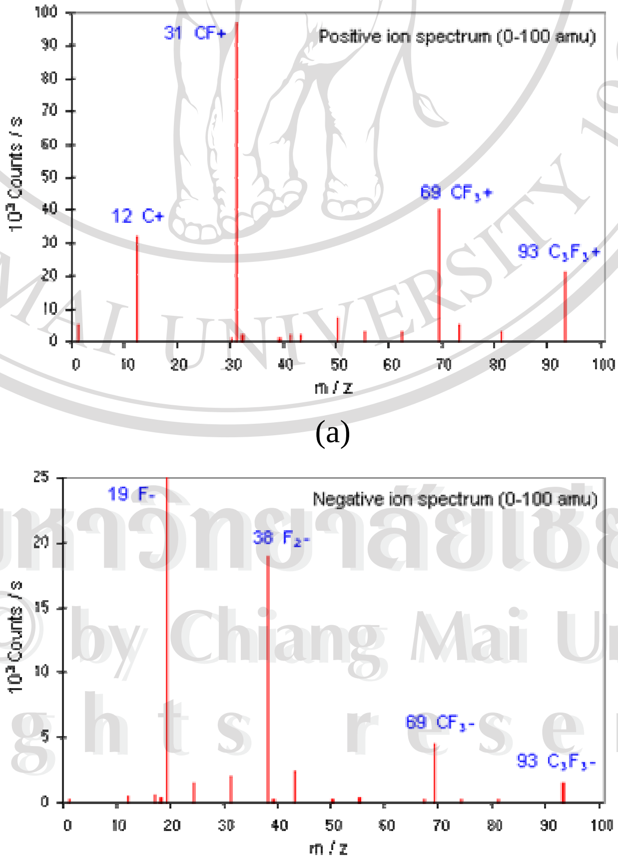

(a)

(b)

Figure 2.22 Mass spectra of polytetrafluoroethylene (a) positive ion spectrum (b) negative ion spectrum (Roger, 2003).

2.4.2 Depth profiling

The depth profiling is the variation of composition with depth below the initial surface. This information is useful for the analysis of layer structures. Sample surface is eroded by the incident ion beam probe then the secondary ions are counted. The count rate as a function of time leads to depth profiles. The raw data for a measurement of phosphorous in a silicon matrix are shown in Figure 2.23. The sample was prepared by implanted phosphorous into a silicon wafer (Fleming, 1995). Cs+ is the primary ions bombarding to the sample and secondary ions are negative.

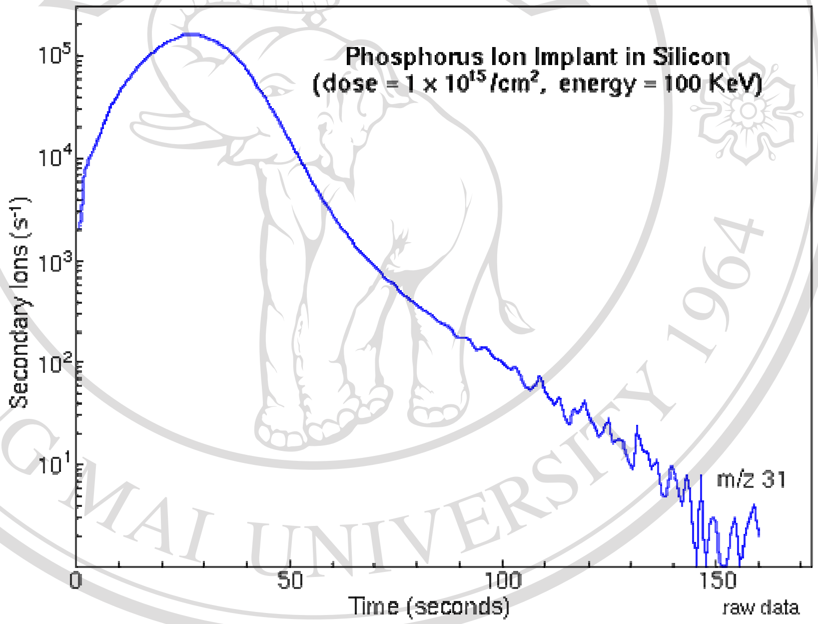

Figure 2.23 The count rate of secondary ions as a function of time (Fleming, 1995).

The time axis is converted into depth by using a profilometer to measure the sputter crater depth (Fleming, 1995). A profilometer is a separate instrument that determines depth by dragging a stylus across the crater and noting vertical deflections. The profilometry gives 0.74 μm for the the above phosphorous depth profile. Total crater depth divided by total sputter time provides the average sputter rate. The vertical axis is converted to concentration using the relative sensitivity factors (RSF).

Quantitative analysis by SIMS uses relative sensitivity factors defined according to Equation 2.34.

$$\frac{I_R}{C_R} = RSF_E \bullet \frac{I_E}{C_E} \tag{2.34}$$

where RSF_E is relative sensitivity factor of element E, I_E is the secondary ion intensity for element E, I_R is the secondary ion intensity for reference element R, C_E is the concentration of element E and C_R is the concentration of referrence element R. The major (matrix) element is usually chosen as the reference. Equation 2.34 gives rise to

$$RSF = C_M \bullet RSF_E \tag{2.35}$$

when

$$RSF = \frac{C_E I_R}{I_E} \tag{2.36}$$

The RSF value for the phosphorous is 1.07x10^{23} atoms/cm^3 and the matrix current (I_R) is 2.2x10^8 silicon ion counts per second. Figure 2.24 shows the phosphorous depth profile.

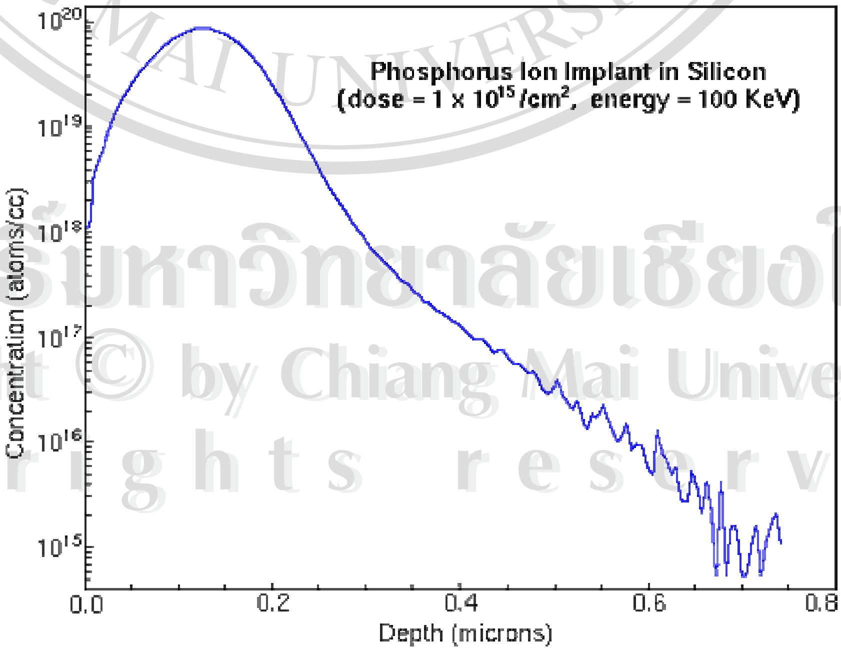

Figure 2.24 Depth profile of phosphorus implant to silicon wafer (Fleming, 1995).